

# Red/Blue shifts of photons in a Hayward black hole immersed in perfect fluid dark matter

L. Marlene. López\* and L. A. López†

*Área Académica de Matemáticas y Física,*

*UAEH, Carretera Pachuca-Tulancingo Km. 4.5,*

*C P. 42184, Mineral de la Reforma, Hidalgo, México.*

## Abstract

We investigate the red/blue shifts of photons emitted by particles moving along stable circular orbits around a Hayward regular black hole immersed in perfect fluid dark matter (PFDM). The PFDM contribution modifies the horizon structure and shifts the characteristic radii associated with circular motion, including the photon sphere and the ISCO radius. We show that the redshift reaches its minimum in the pure Hayward case and increases for nonzero values of the PFDM parameter, whereas the blueshift exhibits the opposite behavior. We also analyze the black hole shadow and compare the results with the observational constraints from Sgr A\*. Positive values of the PFDM parameter reduce the shadow radius, while negative values produce larger deviations from the Schwarzschild case. These results suggest that frequency shifts and black hole shadows may provide observational signatures of PFDM effects in strong gravitational fields.

PACS numbers: 11.27.+d, 98.62.Gq

---

\*Electronic address: lo281479@uaeh.edu.mx

†Electronic address: lalopez@uaeh.edu.mx (Corresponding-Author)

## I. INTRODUCTION

Following the idea of the limiting-curvature hypothesis that, Hayward [1] constructed a static and spherically symmetric regular black hole (BH) in which the central singularity is replaced by an effective de Sitter core, ensuring that the curvature remains finite at the center. The Hayward BH additionally can be derived from a generic class [2] of solutions of general relativity coupled to nonlinear electrodynamics. These types of regular solutions have been proposed as alternatives to classical black holes in order to overcome the singularity problem in general relativity.

Various extensions of the Hayward solution have been developed to explore a wide range of space-time properties. Among these efforts are studies on the quasi-normal modes of the Hayward black hole [3],[4], analyses incorporating rotation [5], and investigations of the Hayward black hole surrounded by quintessence [6], [7], [8] to mention a few.

The quasi-normal modes of the Hayward black hole immersed in perfect fluid dark matter (Hayward-PFDM) have recently been investigated [9]. This class of models is particularly relevant, as it allows one to explore how the presence of dark matter which is estimated to constitute about 27% of the total energy content of the Universe, modifies observable black holes properties.

The red/blue shifts of photons emitted by particles orbiting compact objects provide an effective tool for probing black hole properties and for proposing new models or methods to determine physical parameters from directly observable quantities. Previous studies have shown that these frequency shifts can be used to extract information of the mass, spin [10] and charge [11] on the black hole. The redshift and blueshift of a black hole immersed in a strong magnetic field [12] as well as those of black holes in nonlinear electrodynamics [13], [14] have also been studied. In a related context, a charged black hole immersed by PFDM has been analyzed in order to study the red/blue shifts of light from orbiting particles the black hole [15].

In addition to frequency shifts, black hole shadows have become one of the most important observational tools for testing gravity in the strong-field regime. The Event Horizon Telescope (EHT) observations of M87\* (2019) [16] and Sgr A\* [17] provide direct information about of space-time near BH. Since the shadow boundary is determined by unstable photon orbits, it is highly sensitive to modifications of the gravitational field produced by

surrounding matter distributions.

Motivated by the above considerations, we analyze the red/blue shifts of photons emitted by particles moving along stable circular orbits around a Hayward-PFDM. In particular, we investigate how the PFDM parameter modifies the horizon structure, the characteristic radii of circular motion, and the resulting observable frequency shifts. Also we investigated the shadow of the Hayward-PFDM black hole.

This article is organized as follows. In Sec. II, we introduce the Hayward-PFDM and briefly analyze its horizon structure. In Sec. III, we examine the stable circular orbits allowed by Hayward-PFDM. In Sec. IV, we determine the frequency shifts of photons emitted by particles moving along stable geodesics in the Hayward-PFDM. Also, in Sec. IV, we analyzed the shadow of the Hayward-PFDM black hole and discussed its dependence on the model parameters. Finally, the conclusions are given in the last section.

## II. HAYWARD BLACK HOLE IMMERSSED IN PERFECT FLUID DARK MATTER

Using the limiting curvature hypothesis and a minimal regularization scheme, Hayward [1] introduced a regular, static, spherically symmetric space-time intended to represent a regular black hole. In this construction, the Einstein tensor approaches an effective cosmological term in the central region,  $G_{\mu\nu} \sim -\Lambda g_{\mu\nu}$  as  $r \rightarrow 0$ , with  $\Lambda = 3/\epsilon^2$ . The parameter  $\epsilon$ , which plays the role of a Hubble-like length scale, encodes the central energy density and generates a repulsive core that prevents the occurrence of curvature singularities.

The Hayward metric is given by;

$$ds^2 = -f(r) dt^2 + \frac{dr^2}{f(r)} + r^2 d\theta^2 + r^2 \sin^2 \theta d\phi^2, \quad (1)$$

with

$$f_{\text{Haw}}(r) = 1 - \frac{2Mr^2}{r^3 + 2M\epsilon^2}, \quad (2)$$

here,  $M$  denotes the mass parameter. In the limit  $\epsilon \rightarrow 0$ , the metric (2) reduces to the Schwarzschild solution. The Hayward admits a critical mass  $\bar{M} = (3\sqrt{3}/4)\epsilon$  and a corresponding radius  $\bar{r} = \sqrt{3}\epsilon$  that determine its causal structure: for  $M < \bar{M}$  no horizon is present; for  $M = \bar{M}$  a single horizon appears at  $r = \bar{r}$ ; and for  $M > \bar{M}$  the Hayward BH exhibits two horizons.

The PFDM model was first proposed by Kiselev [18], whose solution introduces a dark matter distribution modeled as a particular anisotropic fluid. Building on this idea, several works have subsequently been developed, exploring different aspects and generalizations [19].

To obtain BHs solutions immersed in PFDM, one may consider the Einstein field equations in the form

$$R_{\mu\nu} - \frac{1}{2}g_{\mu\nu}R = 8\pi (T_{\mu\nu}^{(\text{OR})} \pm T_{\mu\nu}^{(\text{PFDM})}), \quad (3)$$

where  $T_{\mu\nu}^{(\text{OR})}$  denotes the stress-energy tensor of the ordinary matter (if any), and  $T_{\mu\nu}^{(\text{PFDM})}$  represents the PFDM contribution. In the case on PFDM, the energy momentum tensor can be expressed as  $T_{\mu}^{\nu} = \text{diag}(-\rho, p_r, p_{\theta}, p_{\phi})$  where  $\rho$  represent the energy density of dark matter and  $(p_r, p_{\theta}, p_{\phi})$  are the pressures.

In order to solve the Einstein field equations (3), it is assumed a static and spherically symmetric space-time. Under this ansatz, integrating the field equations with the PFDM stress-energy tensor leads to a BH solution whose metric function acquires an additional logarithmic term  $\frac{\alpha}{r} \log(\frac{r}{|\alpha|})$  ([20], [21], [22], [23]), where  $\alpha$  is an integration constant that characterizes the strength of the dark matter distribution.

Following these ideas, we can write the function metric the Hayward (2) black hole immersed in perfect fluid dark matter (Hayward-PFDM) as:

$$f(r) = 1 - \frac{2Mr^2}{r^3 + 2M\epsilon^2} + \frac{\alpha}{r} \log\left(\frac{r}{|\alpha|}\right). \quad (4)$$

Depending on how the tensor  $T_{\mu\nu}^{(\text{PFDM})}$  is incorporated into the Einstein equations (3), the constant  $\alpha$  may be taken to be positive or negative [24] to satisfies the weak energy condition which in turn leads to different BH solutions. This follows from the fact that the energy density associated with the PFDM is related to this parameter  $\alpha$  as  $\rho = \mp\alpha/8\pi r^3$ .

### A. Event horizons

The horizons of Hayward-PFDM are determined by the positive roots of (4). If we then rescale the black hole mass  $M$ , the radial distance  $r$  and the parameter  $\epsilon$  as:  $r \rightarrow r/|\alpha|$ ,  $M \rightarrow M/|\alpha|$ ,  $\epsilon \rightarrow \epsilon/|\alpha|$  (these rescalings are used exclusively for the horizon analysis). The event horizons are given by the roots of:

$$2Mr^3 - 2Mr\epsilon^2 + 2\tau M\epsilon^2 \log(r) - r^4 - r^3\tau \log(r) = 0. \quad (5)$$

Where  $\tau = \pm 1$  for  $\alpha > 0$  and  $\alpha < 0$  respectively.

It is evident that the number of horizons depends on the values assumed by the parameters of Hayward-PFDM. By applying the method used in [25], [26], one can determine the ranges of the parameters  $M$  and  $\epsilon$  for which horizons exist.

Of (5)  $M$  can be parametrized as a function of  $r$  and  $\epsilon$  as:

$$M(r, \epsilon^2) = \frac{r^3(\tau \log(r) + r)}{2(r^3 - \tau\epsilon^2 \log(r) - r\epsilon^2)}, \quad (6)$$

then  $M(r, \epsilon^2)$  (6) has extrema ( $dM(r, \epsilon)/dr = 0$ ) in a  $\epsilon^2(r)$ :

$$\epsilon^2(r) = \frac{(r + \tau)r^3}{3(r + \tau \log(r))^2}. \quad (7)$$

The function  $\epsilon^2(r)$  (7) exhibits a critical (minimum) values at  $r_{crit} = 1.09759$  (for  $\alpha > 0$ ) and  $r_{crit} = 0.774652$  (for  $\alpha < 0$ ). A detailed analysis shows that  $\epsilon^2(1.09759) = (\epsilon_{crit}^2)_{\alpha > 0} = 0.65209$  and  $\epsilon^2(0.774652) = (\epsilon_{crit}^2)_{\alpha < 0} = -0.0329142$ , however  $\epsilon^2$  must be positive then we consider that  $(\epsilon_{crit}^2)_{\alpha < 0} = 0$ .

The critical values for  $M(r, \epsilon^2)$  are obtained by evaluating (6) at the critical values, obtaining that  $(M_{crit})_{\alpha > 0} = 1.44227$  (minimum) and  $(M_{crit})_{\alpha < 0} = 0.514997$  (minimum).

In summary, for  $\epsilon_{crit}^2 \leq \epsilon^2$  and  $M_{crit} \leq M$  the Hayward-PFDM has horizons.

We next consider the case extreme when  $df(r)/dr = 0$  and  $f(r) = 0$  are satisfied simultaneously, where it is possible to obtain the following reaction:

$$M(r) = \frac{3(\tau \log(r) + r)^2}{6\tau \log(r) + 4r - 2\tau}. \quad (8)$$

In Fig. 1, the dependence of  $M$  as a function of  $\epsilon^2$  is presented using the equations (7) and (8). For  $\alpha > 0$ , the number of horizons increases and the Hayward-PFDM black hole may exhibit up to three horizons (region I in Fig. 1a)), a feature also reported for black holes surrounded by dark energy [27],[28],[29]. The boundaries between regions I and II correspond to extremal configurations with two horizons, while region II corresponds to solutions with a single horizon.

Fig. 1 b) present the case  $\alpha < 0$ , in region I the Hayward-PFDM has two horizons, while in region II there are no horizons. The boundaries of regions I and II represent the extreme

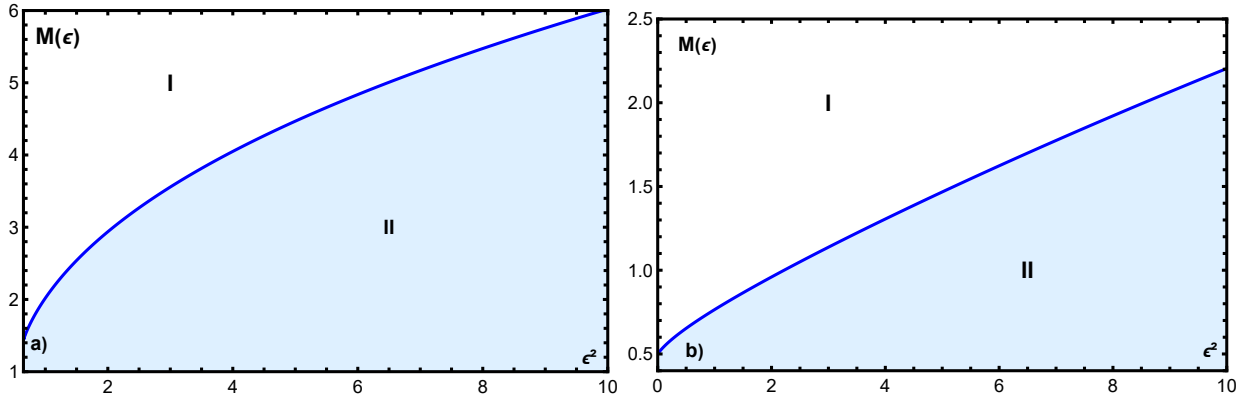


FIG. 1: The figures show the behavior of  $M$  as function of  $\epsilon^2$ . a) For  $\alpha > 0$ , the region I contain the values of  $M$  and  $\epsilon^2$  so that Hayward-PFDM has three horizons, in II Hayward-PFDM has one horizon and the boundary of the regions I and II represents the extremal Hayward-PFDM (two horizon). b) For  $\alpha < 0$ , the region I contain the values of  $M$  and  $\epsilon^2$  so that Hayward-PFDM has two horizons, in II Hayward-PFDM has no horizons and the boundary of the regions I and II represents the extremal Hayward-PFDM (one horizon).

cases of Hayward-PFDM. Depending on the values of the parameters  $M$ , and  $\epsilon^2$  the number of the horizons may decrease from two to one, then when the the PFDM is introduced the number of horizons does not increase.

A comparison of the critical masses shows that a positive PFDM parameter ( $\alpha > 0$ ) increases the critical mass. Specifically, the ordering satisfies  $\bar{M} < (M_{\text{crit}})_{\alpha < 0} < (M_{\text{crit}})_{\alpha > 0}$ .

### III. EFFECTIVE POTENTIAL FOR TEST PARTICLES

As a first step in the determination of the frequency shifts of particles orbiting around a black hole, the effective potential is analysed in order to identify the conditions required for the existence of stable orbits.

For this purpose, we consider a static and axially symmetric space-time, described by Eq. (1) in spherical coordinates, and analyse the motion of test particles through the geodesic equations obtained from the Lagrangian formalism:

$$\mathcal{L} = g_{\mu\nu}U^\mu U^\nu, \quad (9)$$

where  $U^\mu = \frac{dx^\mu}{d\tau}$  is the four-velocity and  $\tau$  is an affine parameter. The condition  $\mathcal{L} = 0$  corresponds to null geodesics (photons), whereas  $\mathcal{L} = -1$  characterizes the trajectories of massive particles.

The conserved quantities associated with the motion of massive particles are the energy  $E$  and the angular momentum  $L$ , which are given by:

$$E = -f(r)U^t, \quad L = r^2 \sin \theta U^\phi. \quad (10)$$

For equatorial orbits ( $\theta = \pi/2$ ), the radial equation of motion for a massive particle in the static space time  $(U_r)^2 + V_{\text{eff}} = E^2$ , where  $V_{\text{eff}}$  denotes the effective potential governing the radial motion:

$$V_{\text{eff}} = \left(1 + \frac{L^2}{r^2}\right) f(r). \quad (11)$$

For the Hayward-PFDM, the effective potential describing the radial motion of massive particles is given by;

$$V_{\text{eff}} = \frac{A(L^2 + r^2) + r^4(L^2 - 2Mr^5) + LB}{r^3(2M\epsilon^2 + r^3)}, \quad (12)$$

where  $A = \alpha(2M\epsilon^2 + r^3) \log\left(\frac{r}{|\alpha|}\right)$  and  $B = 2Mr(\epsilon^2 - r^2)$ .

In Fig. 2 a), we show the behavior of the effective potential  $V_{\text{eff}}$ , Eq.(11), for the Hayward-PFDM considering different values of  $\alpha > 0$ . The effective potential exhibits both a maximum and a minimum, indicating the presence of unstable and stable circular orbits, respectively, the plot also shows that the motion of test particles is noticeably affected by the PFDM parameter. In particular, as  $\alpha$  increases, the maximum of the effective potential shifts toward the horizon, whereas the minimum is displaced in the opposite direction.

In panel b) of the Fig. 2, the behavior of  $V_{\text{eff}}$  is shown considering different values of  $\alpha < 0$ . The behavior is similar to that displayed in panel a) (see Fig. 2), exhibiting both a maximum and a minimum. However, the maximum of the potential are lower for  $\alpha < 0$ , indicating that the gravitational effect is stronger in the presence of the parameter  $\alpha > 0$ , which highlights the importance of considering the PFDM contribution.

We note that the existence of extrema (both maxima and minima) of the effective potential is constrained by the angular momentum  $L$ . In particular, the formation of minima for  $\alpha > 0$  requires smaller values of  $L$  than those corresponding to  $\alpha < 0$ . Additionally, the

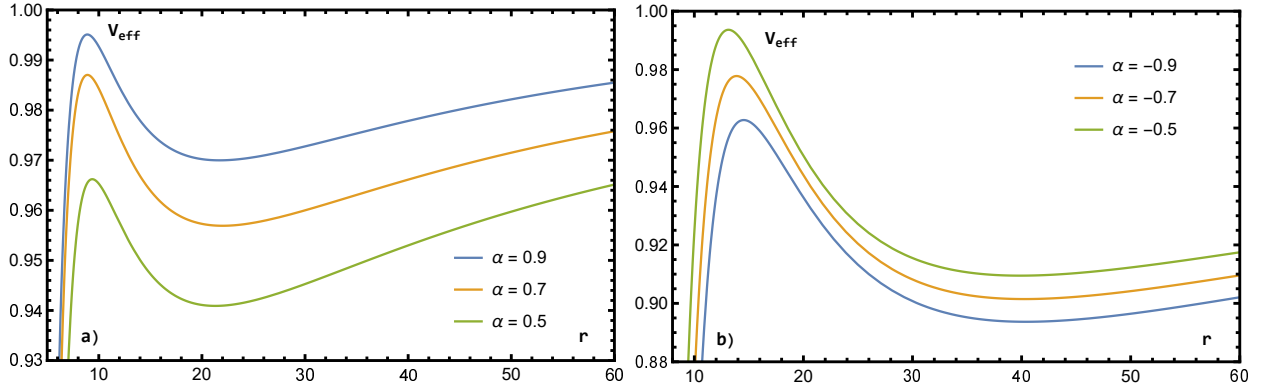


FIG. 2: a) Behavior of the effective potential  $V_{\text{eff}}$  for different values of the PFDM parameter  $\alpha > 0$  with angular momentum  $L = 6.8$ . b) Behavior of the effective potential  $V_{\text{eff}}$  for different values of the PFDM parameter  $\alpha < 0$  with angular momentum  $L = 14$ . In both panels, we consider  $M = 2.7$  and  $\epsilon = 0.85$ .

radii of stable circular orbits increase as  $\alpha$  increases, suggesting that the presence of perfect fluid dark matter shifts the region of stable motion toward larger radial distances.

#### IV. ORBITS AROUND A HAYWARD-PFDM

Before analysing the red/blue shifts of photons emitted by massive particles orbiting the Hayward-PFDM black hole, it is necessary to first analyse the possible orbits that can exist. We restrict our analysis to circular orbits. Such trajectories must satisfy the conditions  $V_{\text{eff}}(r) = E^2$  and  $V'_{\text{eff}}(r) = 0$ , the prime indicates differentiation with respect to the radial coordinate  $r$ . For circular orbits to be stable  $r_c$ , it is additionally required that  $V''_{\text{eff}}(r_c) > 0$  ensure that small radial perturbations do not lead to deviations from the circular trajectory.

Therefore, we can derive the following expressions [30] for the energy and angular momentum of a particle in circular orbits:

$$E^2 = \frac{2f^2(r)}{2f(r) - rf'(r)}, \quad L^2 = \frac{r^3 f'(r)}{2f(r) - rf'(r)}. \quad (13)$$

Then (13) in terms of Hayward-PFDM is given by;

$$E^2 = \frac{4\alpha(A + B + r^4)^2}{r(3A^2 - 2\alpha(\alpha - 2r)(4M^2\epsilon^4 + r^6) + 2Mr^3(2\alpha\epsilon^2 + 3r^3 - 4r\epsilon^2))}, \quad (14)$$

and

$$L^2 = \frac{r^2 (-A^2 + 2\alpha (4\alpha M^2 \epsilon^4 + r^6 (\alpha + 2M) + 4Mr^3 \epsilon^2 (\alpha - 2M)))}{3A^2 - 2\alpha (\alpha - 2r) (4M^2 \epsilon^4 + r^6) + 2Mr^3 (2\alpha \epsilon^2 + 3r^3 - 4r\epsilon^2)}. \quad (15)$$

One finds that circular orbits do not exist for arbitrary values of  $r$ . In particular, when the energy (14) diverges, the corresponding trajectory describes a photon orbit, also known as the photosphere radius ( $r_{\text{ph}}$ ). Thus, the photosphere radius is obtained by setting the denominator of (14) to zero.

The marginally bound circular orbits ( $r_{\text{mb}}$ ) are characterized by the condition  $E = 1$ , while the innermost stable circular orbits (ISCO) are determined by the requirement  $V_{\text{eff}}''(r) = 0$  in  $r = r_{\text{ISCO}}$  given by:

$$rf(r)f''(r) + 3f(r)f'(r) - 2r(f'(r))^2 = 0, \quad (16)$$

in terms of the Hayward–PFDM (16) is given by;

$$A^4(-4\alpha + r + 3) + 4\alpha^3 (\alpha P_1 + 4Ar^3 M (22M^2 \epsilon^4 + 11Mr^3 \epsilon^2 - 3r^6) + P_0 + \alpha^2 P_2) = 0, \quad (17)$$

with  $P_1 = 8Mr^3 (r^3 - 4M\epsilon^2) (2M\epsilon^2 + r^3)^2$ ,  $P_2 = 2 (2M\epsilon^2 + r^3)^4$  and

$$P_0 = 2Mr^4 (32M^3 \epsilon^6 + 4M^2 r^2 \epsilon^4 (8M + 13r) + r^8 (6M - r) + 4Mr^5 \epsilon^2 (4r - 17M)). \quad (18)$$

The comparison of the different orbits is shown in Fig.(3), the photon sphere  $r_{\text{ph}}$ , the marginally bound orbit  $r_{\text{mb}}$ , and the ISCO radius  $r_{\text{ISCO}}$ . The different orbits depend on the parameter  $\alpha$ .

In Fig. 3 a) ( $\alpha > 0$ ), all radii decrease monotonically with  $\alpha$  increase, preserving the relation  $r_{\text{ph}} < r_{\text{mb}} < r_{\text{ISCO}}$ . This behavior indicates that the presence of PFDM shifts the region of stable motion inward, effectively increasing the gravitational attraction at intermediate scales and requiring minors orbital radii to sustain stable circular orbits.

In contrast, Fig. 3 b) ( $\alpha < 0$ ) exhibits the same ordering  $r_{\text{ph}} < r_{\text{mb}} < r_{\text{ISCO}}$ , but all radii increase monotonically with increasing  $|\alpha|$ . In this regime, the characteristic radii decrease as  $\alpha \rightarrow 0$ .

In the limit  $\alpha \rightarrow 0$ , both branches smoothly converge to the pure Hayward solution, confirming that PFDM acts as a continuous deformation of the space-time. Therefore,

the parameter  $\alpha$  governs the displacement of circular orbits and plays a central role in determining the orbital dynamics and the associated observable effects.

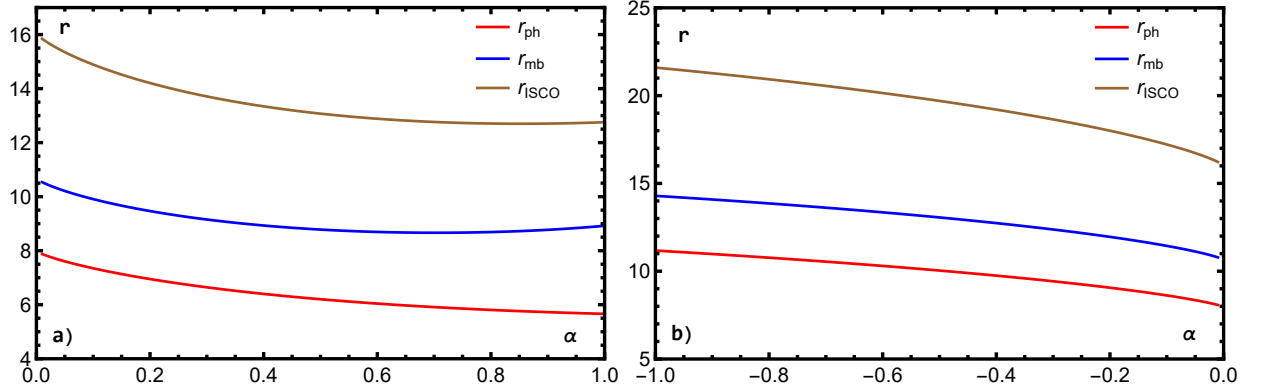


FIG. 3: Behavior of the photon sphere radius  $r_{\text{ph}}$ , the marginally bound orbit radius  $r_{\text{mb}}$ , and the innermost stable circular orbit radius  $r_{\text{ISCO}}$  as functions of the PFDM parameter  $\alpha$ , for fixed values of  $M = 2.7$  and  $\epsilon = 0.85$ . Panel a) corresponds to  $\alpha > 0$ , while panel b) corresponds to  $\alpha < 0$ .

## V. THE RED/BLEUE SHIFTS FOR PHOTON

The relationship between the red/blue shifts of photons emitted by massive particles (such as stars or gas) moving along stable geodesics around a black hole was first highlighted in [10]. Subsequently, the same method was developed for static space-times in [30].

Now to proceed with the analysis, we consider a photon emitted by particles orbiting the Hayward-PFDM black hole in stable circular orbits of radius  $r_c$  and moving in the same equatorial plane,  $\theta = \pi/2$ . The four-momentum of the photon is denoted by  $K^\mu$ , which satisfies the null condition  $K^\mu K_\mu = 0$ . Moreover, the photon energy and angular momentum are conserved quantities, given by;

$$E_{ph} = -f(r) K^t, \quad L_{ph} = r^2 K^\phi. \quad (19)$$

Now, the frequency shift  $z$  associated with the 4-velocity of emission ( $e$ ) and the 4-velocity of detection ( $d$ ) of the photon is given by  $1 + z = \omega_e/\omega_d$  where  $\omega_{e,d}$  are the frequencies given by;

$$\omega_e = -K_\mu U_e^\mu, \quad \omega_d = -K_\mu U_d^\mu. \quad (20)$$

For particles moving along circular geodesics  $U_r = 0$  and equatorial motion  $U_\theta = 0$ ;

$$\omega_e = E_{ph}U_e^t - L_{ph}U_e^\phi, \quad \omega_d = E_{ph}U_d^t - L_{ph}U_d^\phi. \quad (21)$$

Hence the frequency shift  $z$  can simplify in the following expression:

$$1 + z = \frac{U_e^t - b_e U_e^\phi}{U_d^t - b_d U_d^\phi}, \quad (22)$$

where the impact parameter  $b = \frac{L_{ph}}{E_{ph}}$  is introduced. Owing to the conservation of energy and angular momentum, the impact parameter remains invariant along the trajectory, implying that  $b_e = b_d$ .

Observational frequency shifts are commonly expressed in terms of energy kinematic frequency shift,  $z_{\text{kin}} = z - z_c$ , where  $z_c$  corresponds to a photon emitted by a static particle with  $b = 0$ . In the case where the detector is located far away from the black hole ( $r \rightarrow \infty$ ), the detector four-velocity becomes  $U_d^\mu = (1, 0, 0, 0)$ , which allows us to obtain the following expression (23);

$$z_{\text{kin}} = U_e^\phi b_{e\pm} = \pm \sqrt{\frac{r f'(r)}{f(r) (2f(r) - r f'(r))}}. \quad (23)$$

The positive sign corresponds to the redshift ( $z_{\text{red}}$ ), while the negative sign corresponds to the blueshift ( $z_{\text{blue}}$ ). Then (23) in terms of Hayward-PFDM is given by;

$$z_{\text{kin}} = \pm \sqrt{\frac{L^2 r^2 (2M\epsilon^2 + r^3)}{A + B + r^4}}. \quad (24)$$

Choosing appropriate values of  $r_c > r_{\text{ISCO}}$ , and using the parameter ranges displayed in Fig. 1, we analyse the kinematic frequency shift  $z_{\text{kin}}$  for the Hayward-PFDM black hole. The results are shown in Fig. 4 for positive and negative values of the PFDM parameter  $\alpha$ .

For  $\alpha > 0$  (Fig. 4 a)), the redshift decreases as  $\alpha$  increases, whereas the blueshift becomes less negative. This means that, in this branch, the PFDM contribution reduces the magnitude of the frequency shift as  $\alpha$  grows. However, the redshift remains above the value obtained for the pure Hayward black hole, whose minimum is reached at  $\alpha = 0$ . Therefore, any nonzero PFDM contribution produces  $z_{\text{red}}^{\text{Hayward-PFDM}} > z_{\text{red}}^{\text{Hayward}}$ .

For  $\alpha < 0$  (see Fig. 4 b)), the same qualitative tendency is observed as  $\alpha$  approaches zero, the redshift decreases and the blueshift increases toward zero. Nevertheless, the magnitudes

of both shifts are larger than those obtained in  $\alpha > 0$ . In particular, negative values of  $\alpha$  enhance the absolute value of the blueshift, indicating a stronger kinematic contribution to the photon frequency variation.

Thus, Fig. 4 shows that the sign of  $\alpha$  has a direct impact on the observable frequency shifts. Positive values of  $\alpha$  tend to reduce the magnitude of both the red/blue shifts as  $\alpha$  increases, whereas negative values produce larger frequency-shift magnitudes. This behavior indicates that red/blue shifts measurements from particles orbiting compact objects may provide a possible observational signature of the PFDM contribution in the space-time.

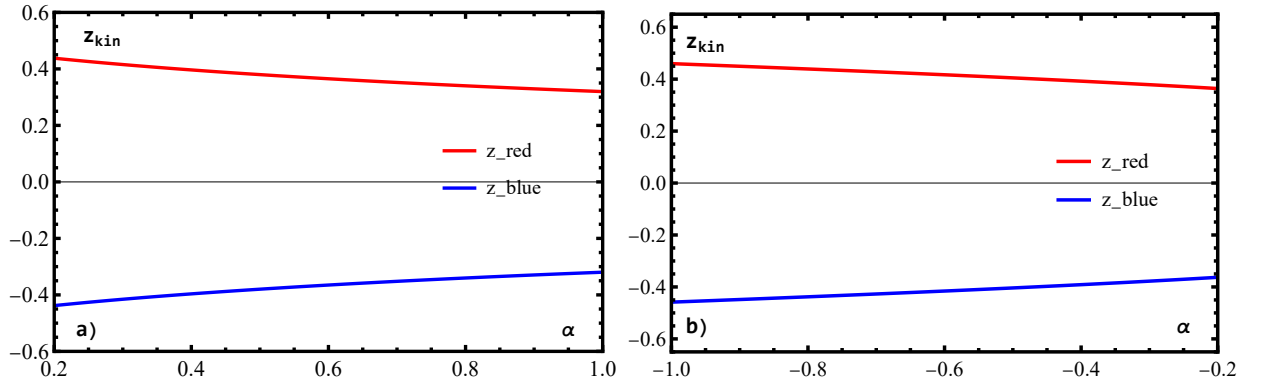


FIG. 4: The figure a) shows the behavior of  $z_{kin}$  as function of  $\alpha > 0$  with  $r = 22$ ,  $\epsilon = 0.85$  and  $M = 2.7$ . In b) shows the behavior of  $z_{kin}$  as function of  $\alpha < 0$  with  $r = 38$ ,  $\epsilon = 0.85$  and  $M = 2.7$ .

## VI. SHADOW OF THE BLACK HOLE

The results of the Event Horizon Telescope (EHT) collaboration have significantly advanced the study of black hole shadows. In particular, the images of M87\* (2019) [16] and Sgr A\* [17] provide direct observational evidence of the space-time geometry near these objects. The black hole shadow corresponds to the dark region formed by photon capture, whose boundary is determined by unstable spherical photon orbits. For a distant observer in a static and spherically symmetric space-time, the shadow radius can be obtained within the optical approximation, where it coincides with the critical impact parameter  $b_c$ , as;

$$r_{sh} = b_c = \sqrt{\frac{r_o^2}{f(r_o)}}, \quad (25)$$

where  $r_o$  denotes the radius of the photon sphere ( $r_{ph}$ ). To confront the Hayward–PFDM black hole with observational data from Sgr A\*, one employs the mass-to-distance ratio, together with a calibration factor that relates the observed emission ring to the actual shadow size. This factor is expected to be close to unity under reasonable astrophysical assumptions. Consequently, one can define the relative deviation  $\delta$  with respect to the Schwarzschild shadow radius:

$$(r_{sh})_{Schw} = 3\sqrt{3}M(1 + \delta), \quad (26)$$

where  $M$  denotes the Schwarzschild mass. Assuming a Gaussian distribution, the corresponding constraints on  $\delta$  are  $0.005 \lesssim \delta \lesssim 0.125$  at the  $1\sigma$  confidence level and  $0.07 \lesssim \delta \lesssim 0.19$  at the  $2\sigma$  confidence level.

The behavior of the shadow radius shown in Fig. 5 reveals the dependence on the PFDM parameter  $\alpha$ . For  $\alpha > 0$  (Fig. 5 a)), the shadow radius decreases monotonically as  $\alpha$  increases, approaching the observational bounds inferred from the EHT observations of Sgr A\*. This behavior indicates that positive PFDM contributions reduce the effective size of the photon capture region, shifting the photon sphere toward smaller radii.

In contrast, for  $\alpha < 0$  (Fig. 5 b)), the shadow radius becomes significantly larger than the Schwarzschild value for large negative  $\alpha$ . As  $\alpha \rightarrow 0$ , the shadow radius decreases and gradually approaches the pure Hayward limit.

Therefore, only a restricted range of the PFDM parameter is compatible with the observational constraints of Sgr A\* at the  $1\sigma$  and  $2\sigma$  confidence levels.

## VII. CONCLUSIONS

In this paper, we have investigated the red/blue shifts of photons emitted by massive particles moving along stable circular orbits around Hayward black hole immersed in perfect fluid dark matter. The horizon analysis revealed that the PFDM parameter changes the number of horizons. For  $\alpha > 0$ , the Hayward-PFDM black hole may exhibit up to three horizons, whereas for  $\alpha < 0$  admits at most two horizons. In both cases, the critical values of the parameters depend strongly on the PFDM contribution, showing that the surrounding dark matter distribution modifies the black-hole geometry.

The effective potential analysis showed the existence of stable and unstable circular orbits

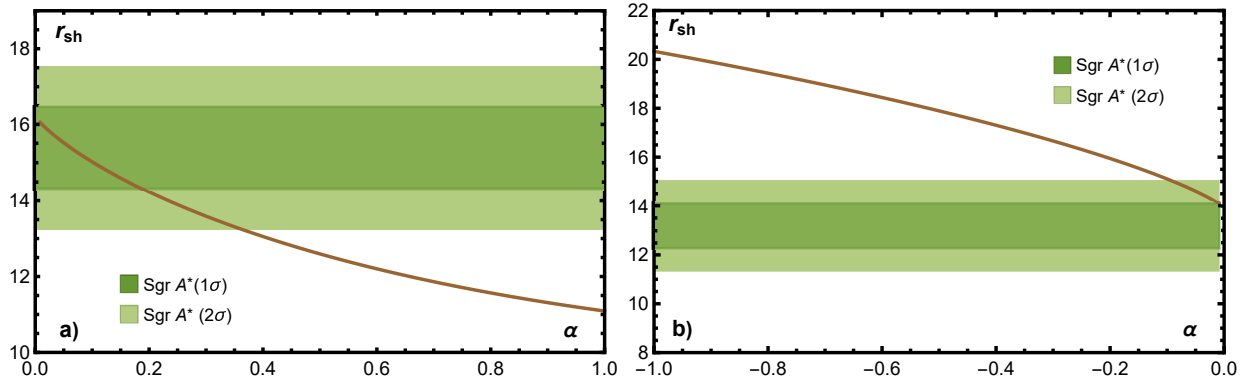


FIG. 5: Shadow radius of the Hayward-PFDM black hole as a function of the PFDM parameter  $\alpha$ : (a)  $\alpha > 0$  and (b)  $\alpha < 0$ . The results are compared with the shadow radius of the Schwarzschild BH. The dark and light green bands represent the observational constraints at the  $1\sigma$  and  $2\sigma$  confidence levels, respectively, derived from the Sgr A\* black hole observations. The parameters are fixed to  $M = 2.27$  and  $\epsilon = 0.85$ .

for both positive and negative values of  $\alpha$ . In particular, the PFDM parameter changes the location of the extrema of the effective potential, indicating that the motion of test particles is sensitive to the dark matter environment.

We also found that the characteristic radii associated with circular motion, namely the photon sphere  $r_{ph}$ , the marginally bound orbit  $r_{mb}$ , and the ISCO radius  $r_{ISCO}$ , preserve the ordering  $r_{ph} < r_{mb} < r_{ISCO}$ , although their magnitudes depend on the sign and value of  $\alpha$ .

Regarding the observable frequency shifts, we found that the redshift reaches its minimum value in the pure Hayward case ( $\alpha = 0$ ). For nonzero values of  $\alpha$ , the PFDM contribution modifies both the red/blue shifts, with different behaviors depending on the sign of the parameter. Positive values of  $\alpha$  tend to reduce the magnitude of the shifts as  $\alpha$  increases, while negative values lead to larger frequency-shift magnitudes. These results indicate that the PFDM environment produces measurable modifications in the propagation of photons emitted near black holes.

In particular, the dependence of the frequency shifts on the sign and magnitude of  $\alpha$  suggests that these observables may help to distinguish different dark matter configurations surrounding compact objects.

Finally, it is worth mentioning that the shadow of the Hayward–PFDM black hole was analyzed, revealing that the PFDM parameter significantly affects its size. Positive values

of  $\alpha$  decrease the shadow radius, whereas negative values lead to larger deviations from the Schwarzschild case. Comparison with the observations of Sagittarius A\* by the Event Horizon Telescope Collaboration suggests that the black hole shadow may provide observational constraints on the PFDM parameter.

## ACKNOWLEDGMENT

L. A. López acknowledges to SECIHTI-SNII, Mexico. Laura Marlene López gratefully acknowledges the financial support provided by SECIHTI through the Masters Fellowship. CVU No 2088339

- 
- [1] Sean A. Hayward. Formation and evaporation of regular black holes. *Phys. Rev. Lett.*, 96:031103, 2006.
  - [2] Zhong-Ying Fan and Xiaobao Wang. Construction of regular black holes in general relativity. *Phys. Rev. D*, 94:124027, Dec 2016.
  - [3] L. A. Lopez and Valeria Hinojosa. Quasinormal modes of Charged Regular Black Hole. *Can. J. Phys.*, 99(1):44–48, 2021.
  - [4] Kai Lin, Jin Li, and Shuzheng Yang. Quasinormal Modes of Hayward Regular Black Hole. *Int. J. Theor. Phys.*, 52:3771–3778, 2013.
  - [5] Muhammed Amir and Sushant G. Ghosh. Rotating Hayward’s regular black hole as particle accelerator. *JHEP*, 07:015, 2015.
  - [6] Omar Pedraza, L. A. López, R. Arceo, and I. Cabrera-Munguia. Geodesics of Hayward black hole surrounded by quintessence. *Gen. Rel. Grav.*, 53(3):24, 2021.
  - [7] Ahmad Al-Badawi and Amani Kraishan. Dirac perturbations of Hayward black hole with quintessence: Quasinormal modes and greybody factor. *Chin. J. Phys.*, 87:59–69, 2024.
  - [8] B. R. Yashwanth, S. K. Narasimhamurthy, Z. Nekouee, and Manjunath Malligawad. Geodesics of Finsler Hayward black hole surrounded by quintessence. *Eur. Phys. J. C*, 84(12):1276, 2024.
  - [9] L. O. Téllez Tovar, Omar Pedraza, L. A. López, and R. Arceo. Quasi-normal modes and absorption section from regular black holes immersed in perfect fluid dark matter. *Mod. Phys. Lett. A*, 41(12n13):2650062, 2026.

- [10] Alfredo Herrera-Aguilar and Ulises Nucamendi. Kerr black hole parameters in terms of the redshift/blueshift of photons emitted by geodesic particles. *Phys. Rev. D*, 92(4):045024, 2015.
- [11] Ricardo Becerril, Susana Valdez-Alvarado, Jose Davila, and Roberto E. Ortega-Miranda. On the relation of the mass, spin and charge parameters with the red and blue shifts of photons emitted by particles orbiting a Kerr–Newman black hole. *Class. Quant. Grav.*, 42(20):205011, 2025.
- [12] L. A. López and Nora Bretón. Redshift of light emitted by particles orbiting a black hole immersed in a strong magnetic field. *Astrophys. Space Sci.*, 366(6):55, 2021.
- [13] L. A. López and J. C. Olvera. Frequency Shifts of photons emitted from geodesics of nonlinear electromagnetic black holes. *Eur. Phys. J. Plus*, 136(1):64, 2021.
- [14] Ricardo Becerril, Susana Valdez-Alvarado, Ulises Nucamendi, Pankaj Sheoran, and J. M. Dávila. Mass parameter and the bounds on redshifts and blueshifts of photons emitted from geodesic particle orbiting in the vicinity of regular black holes. *Phys. Rev. D*, 103(8):084054, 2021.
- [15] Houssam Eddine Trad and Lamine Khodja. Frequency Shift of Photons in Reissner-Nordström Black Hole Immersed in Perfect Fluid Dark Matter. *Int. J. Theor. Phys.*, 64(6):160, 2025.
- [16] Kazunori Akiyama et al. First M87 Event Horizon Telescope Results. I. The Shadow of the Supermassive Black Hole. *Astrophys. J. Lett.*, 875:L1, 2019.
- [17] Kazunori Akiyama et al. First Sagittarius A\* Event Horizon Telescope Results. I. The Shadow of the Supermassive Black Hole in the Center of the Milky Way. *Astrophys. J. Lett.*, 930(2):L12, 2022.
- [18] V. V. Kiselev. Quintessential solution of dark matter rotation curves and its simulation by extra dimensions. 3 2003.
- [19] Ming-Hsun Li and Kwei-Chou Yang. Galactic Dark Matter in the Phantom Field. *Phys. Rev. D*, 86:123015, 2012.
- [20] Sanjar Shaymatov, Daniele Malafarina, and Bobomurat Ahmedov. Effect of perfect fluid dark matter on particle motion around a static black hole immersed in an external magnetic field. *Phys. Dark Univ.*, 34:100891, 2021.
- [21] He-Xu Zhang, Yuan Chen, Tian-Chi Ma, Peng-Zhang He, and Jian-Bo Deng. Bardeen black hole surrounded by perfect fluid dark matter. *Chin. Phys. C*, 45(5):055103, 2021.
- [22] G. Abbas and R. H. Ali. Thermal fluctuations, quasi-normal modes and phase transition of

- the charged AdS black hole with perfect fluid dark matter. *Eur. Phys. J. C*, 83(5):407, 2023.
- [23] Javlon Rayimbaev, Sanjar Shaymatov, and Mubasher Jamil. Dynamics and epicyclic motions of particles around the Schwarzschild–de Sitter black hole in perfect fluid dark matter. *Eur. Phys. J. C*, 81(8):699, 2021.
- [24] Anish Das, Ashis Saha, and Sunandan Gangopadhyay. Study of circular geodesics and shadow of rotating charged black hole surrounded by perfect fluid dark matter immersed in plasma. *Class. Quant. Grav.*, 39(7):075005, 2022.
- [25] Bobir Toshmatov, Zdeněk Stuchlík, and Bobomurat Ahmedov. Rotating black hole solutions with quintessential energy. *Eur. Phys. J. Plus*, 132(2):98, 2017.
- [26] L. A. López and Omar Pedraza. Effects of quintessence on scattering and absorption sections of black holes. *Indian J. Phys.*, 97(1):285–294, 2023.
- [27] Valeria Ramírez, L. A. López, Omar Pedraza, and V. E. Ceron. Scattering and absorption cross sections of Schwarzschild–anti-de Sitter black hole with quintessence. *Can. J. Phys.*, 100(2):112–118, 2022.
- [28] Omar Pedraza, L. A. López, R. Arceo, and I. Cabrera-Munguia. Quasinormal modes of the Hayward black hole surrounded by quintessence: Scalar, electromagnetic and gravitational perturbations. *Mod. Phys. Lett. A*, 37(09):2250057, 2022.
- [29] Sharmanthie Fernando. Schwarzschild black hole surrounded by quintessence: Null geodesics. *Gen. Rel. Grav.*, 44:1857–1879, 2012.
- [30] Ricardo Becerril, Susana Valdez-Alvarado, and Ulises Nucamendi. Obtaining mass parameters of compact objects from redshifts and blueshifts emitted by geodesic particles around them. *Phys. Rev. D*, 94(12):124024, 2016.